JACS
JOURNAL OF THE AMERICAN CHEMICAL SOCIETY

Article

pubs.acs.org/JACS

One-Step, Facile and Ultrafast Synthesis of Phase- and Size-Controlled Pt−Bi Intermetallic Nanocatalysts through Continuous-Flow Microfluidics

Dongtang Zhang,[†] Fuxiang Wu,[†] Manhua Peng,[†] Xiayan Wang,*[,†] Dingguo Xia,*[,‡] and Guangsheng Guo*[,†]

[†]Beijing Key Laboratory for Green Catalysis and Separation, Department of Chemistry and Chemical Engineering, Beijing University of Technology, Beijing 100124, PR China

[‡]Key Lab of Theory and Technology for Advanced Batteries Materials, College of Engineering, Peking University, Beijing 100871, PR China

Supporting Information

ABSTRACT: Ordered intermetallic nanomaterials are of considerable interest for fuel cell applications because of their unique electronic and structural properties. The synthesis of intermetallic compounds generally requires the use of high temperatures and multiple-step processes. The development of techniques for rapid phase- and size-controlled synthesis remains a formidable challenge. The intermetallic compound Pt_1Bi_2 is a promising candidate catalyst for direct methanol fuel cells because of its high catalytic activity and excellent methanol tolerance. In this work, we explored a one-step, facile and ultrafast phase- and size-controlled process for synthesizing ordered Pt−Bi intermetallic nanoparticles (NPs) within seconds in microfluidic reactors. Single-phase Pt_1Bi_1 and Pt_1Bi_2 intermetallic NPs were prepared by tuning the reaction temperature, and size control was achieved by modifying the solvents and the length of the reaction channel. The as-prepared Pt−Bi intermetallic NPs exhibited excellent methanol tolerance capacity and high electrocatalytic activity. Other intermetallic nanomaterials, such as Pt_3Fe intermetallic nanowires with a diameter of 8.6 nm and Pt_1Sn_1 intermetallic nanowires with a diameter of 6.3 nm, were also successfully synthesized using this method, thus demonstrating its feasibility and generality.

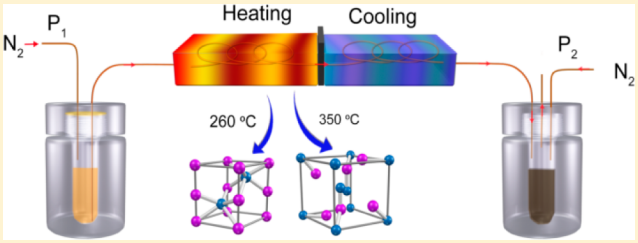

INTRODUCTION

Atomically ordered Pt-based intermetallic nanoparticles (NPs) have been attracting increasing research attention because of their unique electronic and structural properties compared with those of monometallic Pt and conventional alloy catalysts.[1−6] Researchers have devoted considerable efforts to the investigation of Pt-based intermetallic NPs as fuel cell electrocatalysts with the intent of decreasing Pt utilization, increasing catalytic performance and structural stability, and increasing resistance to CO poisoning. Since plenty of works have been conducted by DiSavo, Abruña and colleagues,[1,7−9] Pt−Bi intermetallics (Pt_1Bi_1 and Pt_1Bi_2) are among the most promising candidates for use as fuel cell catalysts because of their high catalytic activity and stability for the oxygen reduction reaction.

A considerable amount of effort has been directed toward the preparation of Pt-based intermetallic NPs for potential use as fuel cell catalysts. The preparation of intermetallic phases typically requires the use of a high-temperature strategy, such as powder metallurgy,[1,7,8] arc melting,[10] sintering,[11] or combustion synthesis.[12] A solution-based synthesis technique has recently been developed that is an attractive strategy for preparing nanoscale intermetallics, but an annealing step is still typically required during or after synthesis.[13−15] Regarding PtBi intermetallics, unsupported ordered intermetallic PtBi nanoparticles have been synthesized using a polyol process,[16] a co-reduction approach,[17] a reduction-based conversion method,[18] and a simultaneous reduction reaction,[19] whereas supported ones have been prepared using the reduction-based conversion method[18] and nucleated-growth synthesis.[2] However, research on the preparation of ordered intermetallic Pt_1Bi_2 nanoparticles is scarce. Xia et al. have reported the synthesis of ordered intermetallic Pt_1Bi_2 nanoparticles on a Vulcan XC-72 carbon support using a co-reduction approach.[20] Because the surface properties of catalysts play a significant role in their catalytic performance, controlling the size and shape of catalysts is critical. However, the reported synthesis methods for Pt−Bi intermetallic NPs still encounter difficulties in the preparation of pure, uniform and monodisperse nanostructures, and these syntheses generally require long stirring, heating, reducing times or an annealing process at high temperatures. Therefore, the development of special chemical synthesis strategies to obtain well-defined Pt−Bi intermetallic NPs is essential.

Received: January 31, 2015
Published: May 1, 2015

DOI: 10.1021/jacs.5b01088
J. Am. Chem. Soc. 2015, 137, 6263−6269

Microfluidic reactor technology for chemical synthesis has rapidly developed because of its unique characteristics, such as its enhanced mixing for reactants, rapid reactions, rapid heat transfer, precise control, and safe operating environment.[21−23] Moreover, multiplexing using parallel capillaries or a microchip with parallel channels can increase the output to realize the scaling up the production.[24,25] The performance of nanomaterials strongly depends on their physical and chemical properties, which are, in turn, related to their particle structures, morphologies and surface properties; therefore, the synthesis of nanomaterials requires considerable control over the reactions. Fortunately, microfluidic reactors can fulfill the requirements for size-, shape-, and structure-controlled syntheses. Microfluidic reactors have come into widespread use for the preparation of a broad variety of nanomaterials, such as metal nanoparticles,[26−31] semiconductor quantum dots,[32−38] and hybrid inorganic nanoparticles.[39−43] However, to the best of our knowledge, the preparation of intermetallic NPs using microfluidic reactors has not yet been reported. Here, we explore the use of microfluidic systems to synthesize intermetallic nanoparticles (NPs), exploiting the superior reaction control offered by such systems.

In this work, we report a simple and rapid method for the synthesis of phase- and size-controlled intermetallic NPs in a single step using continuous-flow microfluidics. The phase control of Pt_1Bi_1 and Pt_1Bi_2 was achieved by simply adjusting the reaction temperature, whereas the size control was easily implemented by regulating the solvents and modifying the length of the reaction channel. The electrochemical results demonstrated that the as-prepared Pt−Bi intermetallic NPs possessed excellent methanol tolerance capacity and exhibited high electrocatalytic activity. Furthermore, the generality of microfluidic reactors for the synthesis of intermetallic nanomaterials was also tested by synthesizing Pt_3Fe and Pt_1Sn_1 nanowires.

EXPERIMENTAL SECTION

Chemicals. Bismuth nitrate ($Bi(NO_3)_3{\cdot}5H_2O$, 99.0%), hexachloroplatinic acid ($H_2PtCl_6{\cdot}6H_2O$, 99.9%), polyvinylpyrrolidone (PVP, K30, 99.9%), ethylene glycol (EG, 99.0%), and polyethylene glycol (PEG400 and PEG600, 99.0%) were purchased from Sinopharm Chemical Reagent Beijing Co., Ltd. The commercial Pt/C (Pt/C, 20 wt %) and Nafion 117 solution (5%) were obtained from Sigma-Aldrich. Ultrapure water (18.2 MΩ cm) was used to prepare the solutions.

Synthesis of Pt−Bi Intermetallic NPs. One hundred milliliters of different polyols was degassed with nitrogen before adding 97 mg of $Bi(NO_3)_3{\cdot}5H_2O$ and 333 mg of PVP in this solution. After $Bi(NO_3)_3{\cdot}5H_2O$ and PVP were dissolved completely, 5 mL of 1% $H_2PtCl_6{\cdot}6H_2O$ (dissolved in ethanol) was added in the mixture to prepare the precursor solutions.

Microfluidic reactor system was connected as shown in Figure 1, and the precursor solution was filled in a sample vial in a PMMA pressure chamber, and introduced to a microfluidic reactor (200 μm i.d.; 365 μm o.d.) by a pressure-regulated nitrogen gas. The length of the microcapillary in the heating region was ∼120 cm, while in the cooling region is ∼10 cm, unless indicated otherwise. A collection vial was put in another PMMA pressure chamber under a certain backpressure at the outlet of the microcapillary. The products were collected by a centrifugation process, and then washed with ethanol. After a drying step at 60 °C overnight, the Pt−Bi intermetallic catalysts were obtained. For preparation of XC-72 supported intermetallic NPs, XC-72 was added to the collected product mixtures and these were stirred for 10 h before the centrifugation process.

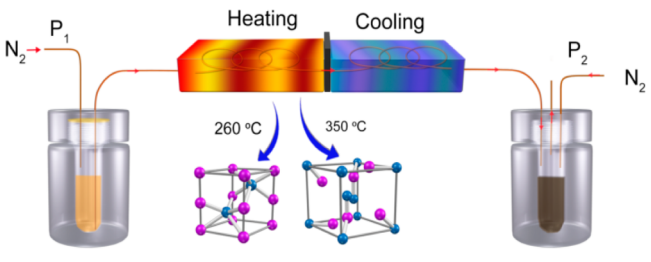

Figure 1. Schematic representation of the microfluidic reactor system.

Characterization of Pt−Bi Intermetallic NPs. Powder X-ray diffraction (XRD) patterns were recorded using a Bruker diffractometer with Cu Kα radiation (D8 Advance X-ray diffractometer, Cu Kα, λ = 1.5406 Å, 40 kV and 40 mA) to study the crystallographic information on the samples. Transmission electron microspectroscopy (TEM) and energy dispersive X-ray spectroscopy (EDS) were carried out with a JEOL JEM-2100 microscope operating at 200 kV with a nominal resolution. High resolution scanning transmission electron microscopy/energy dispersive X-ray microanalysis (HRSTEM/EDX) were performed on JEOL ARM200F with an accelerating voltage of 200 kV. The bulk composition of the prepared intermetallic NPs was measured using inductively coupled plasma-atomic emission spectrometry (ICP-AES).

Electrochemical Measurements. The electrochemical measurements were performed using a VMP3 multichannel potentiostat/galvanostat (Bio-Logic SAS, France) at the room temperature. The glassy carbon rotating disk electrode (GC-RDE, 4 mm diameter) was used as the working electrode. A GC film electrode and a reversible hydrogen electrode (RHE) were used as the counter electrode and the reference electrode, respectively. Before using a GC electrode as a substrate for the intermetallicNPs, it was polished with 0.05 mm alumina to yield a mirror finish and washed before experiment. Then, the ethanol suspensions of the as-prepared concave Pt_1Bi_2/XC-72 or Pt/C NPs were transferred to the surface of the GC electrode and dried at room temperature.

Before measurement, the working electrode loaded with the as-prepared concave catalysts was electrochemically cleaned by continuous potential cycling between 0.0 and 1.2 V at 200 mV/s in 0.10 M H_2SO_4 solution until a stable cyclic CV curve was obtained. The ORR measurements were performed in O_2-saturated 0.1 M $HClO_4$ solutions using GC-RDE at a sweep rate of 10 mV/s under different rotation rate with or without methanol.

RESULTS AND DISCUSSION

Synthesis of Pt−Bi Intermetallic NPs. A schematic representation of the capillary microfluidic system that was used to prepare the Pt−Bi intermetallic NPs is provided in Figure 1. The reaction solutions were driven from a pressure chamber into the microfluidic reactor by pressure-regulated nitrogen gas. The products were collected at the outlet of the microcapillary. The experimental conditions were controlled by a pressure regulator, a downstream back-pressure regulator and segmented regions of precise temperature control. The back-pressure regulator was used to suppress the gasification of solvents under elevated temperatures. One of the two adjacent regions of precise temperature control was designed for heating, and the other, for cooling. When the reaction solution was introduced into the heating region, it was heated to the desired temperature within a very short time because of the rapid heat transfer in the microchannels, and then, the reaction occurred. Subsequently, the products formed in the heating region flowed into the downstream cooling region to quickly terminate the reaction, thus effectively avoiding possible side reactions or particle aggregation. Precise segmented temperature control is challenging in conventional reaction techniques, but it can be easily achieved in microfluidic reactor systems. In

DOI: 10.1021/jacs.5b01088
J. Am. Chem. Soc. 2015, 137, 6263−6269

addition, in a microfluidic system, the reaction solutions and the products collect separately at the two ends of the reactor, thereby allowing for continuous synthesis to ensure good reproducibility of the synthesis process. Moreover, when the reaction solution was flowed through the microfluidic reactor, the products were synthesized and collected immediately, within seconds. Thus, ultrafast preparation of intermetallic NPs was achieved.

We first sought to prepare Pt−Bi intermetallic NPs in the microfluidic reactor to serve as a proof of concept. Pt−Bi intermetallic NPs were formed using $H_2PtCl_6{\cdot}6H_2O$ and $Bi(NO_3)_3{\cdot}5H_2O$ as the metal precursors, ethylene glycol or polyethylene glycol (PEG400 and PEG600) as the solvent and reducing agent, and PVP as the stabilizer. A series of XRD patterns of the products obtained when using ethylene glycol at different reaction temperatures are presented in Figure 2. When

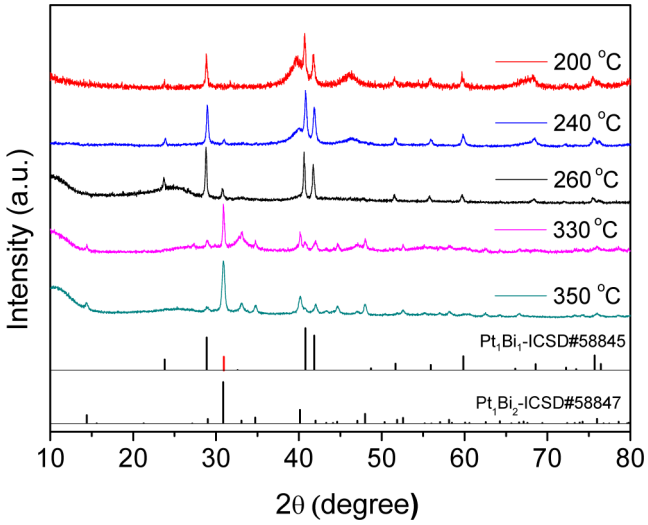

Figure 2. XRD patterns of the products obtained at various reaction temperatures.

the reaction temperature was set to 200 °C, two types of diffraction peaks were observed: the broad peaks at 39.7° and 46.2° can be indexed to pure Pt metal, and the sharp peaks at 28.9°, 32.6°, 40.7°, 41.8°, 55.9°, 59.8° and 68.5° correspond to the Pt_1Bi_1 intermetallic phase. This result indicates the presence of a Pt metal phase and an ordered Pt_1Bi_1 intermetallic phase.

As the reaction temperature was increased from 200 to 260 °C, the broad peaks in the XRD patterns of pure Pt gradually diminished and the sharp peaks of the Pt_1Bi_1 intermetallic phase became dominant, reflecting the formation of particles during the conversion process.[15] The XRD pattern of the product obtained at 260 °C indicates the presence of only a single Pt_1Bi_1 intermetallic phase with a hexagonal structure. When the reaction temperature was further increased to 330 °C, the characteristic diffraction peaks of a Pt_1Bi_2 intermetallic phase with a trigonal structure were observed, indicating that a Pt_1Bi_2 intermetallic phase had formed. As the temperature was further increased to 350 °C, pure Pt_1Bi_2 was obtained. We conclude that increasing the temperature can accelerate the rate of transformation of Pt and Bi into intermetallic phases and that the reaction temperature has a significant effect on the composition of the products. A specific reaction temperature is required for the complete transformation of Pt and Bi elements into various intermetallic phases in this microfluidic reactor.

Figure 3 presents TEM images and high-resolution TEM (HRTEM) images of the as-prepared intermetallic NPs

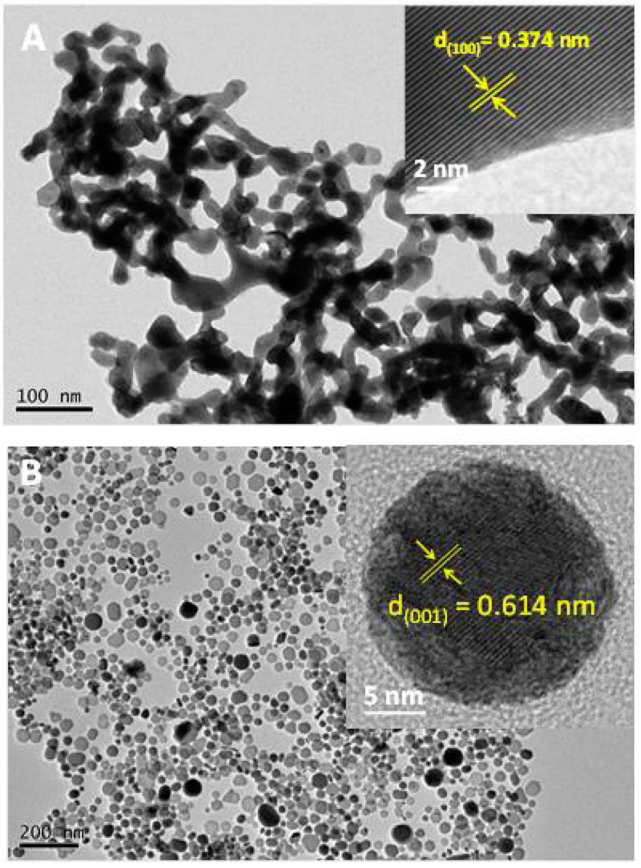

Figure 3. TEM images of Pt_1Bi_1 (A, 260 °C) and Pt_1Bi_2 (B, 350 °C) intermetallic NPs prepared in ethylene glycol.

obtained at 260 and 350 °C. As shown in Figure 3A, the majority of the Pt_1Bi_1 nanocrystals were uniform V-shaped nanorods with an arm diameter of approximately 17 nm that was knit into a nanocrystalline network. The Pt_1Bi_1 intermetallics NPs possessed a crystalline structure, as indicated by the clear lattice fringes observed in the HRTEM image presented in the inset of Figure 3A. The measured lattice fringe distance of 0.374 nm is consistent with the (100) plane of Pt_1Bi_1. Figure 3B presents a TEM image of Pt_1Bi_2 intermetallic nanocrystals prepared at 350 °C; in this image, only nanospherical morphology is observed. The lattice fringe distance was measured to be 0.614 nm, which can be indexed to the (001) plane of Pt_1Bi_2 (the inset of Figure 3B). The chemical composition of the as-prepared intermetallic NPs was determined via EDS. The EDS spectra exhibit average Pt-to-Bi ratios of 51.9:48.1 and 35.2:64.8, which indicate the presence of a Pt_1Bi_1 phase and a Pt_1Bi_2 phase, respectively, in the products (Supporting Informaton Figures S1 and S2). The overall atomic percentages of Bi in the Pt_1Bi_1 NPs and the Pt_1Bi_2 NPs were 50% and 66%, respectively, as determined via ICP-AES. The EDS and ICP-AES results are consistent with the XRD results and further confirm that the products prepared at 260 and 350 °C were pure Pt_1Bi_1 and Pt_1Bi_2 intermetallic NPs, respectively.

DOI: 10.1021/jacs.5b01088
J. Am. Chem. Soc. 2015, 137, 6263−6269

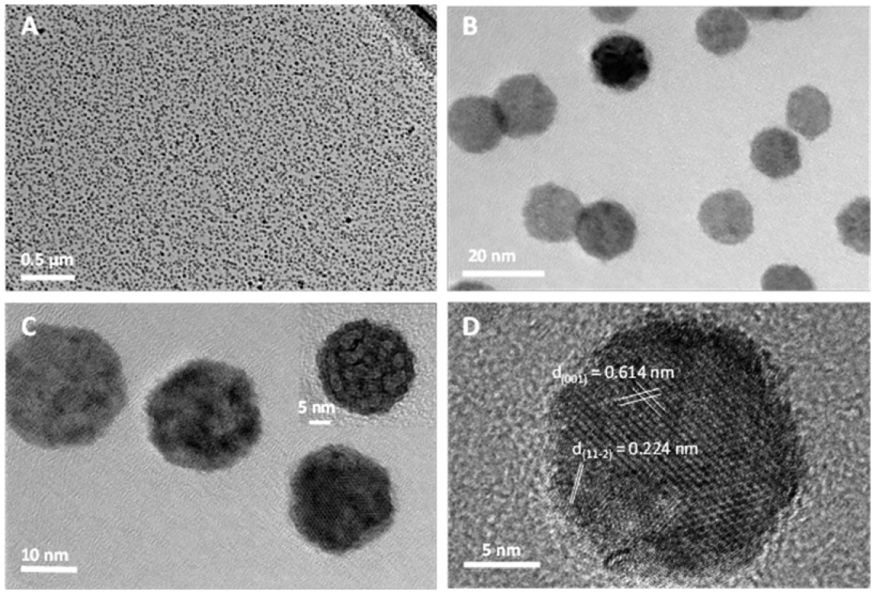

Figure 4. TEM and HRTEM images of Pt_1Bi_2 NPs prepared in PEG600 at 350 °C. (A) TEM image; (B and C) magnified TEM images; (D) HRTEM image of the knitted ball structure of Pt_1Bi_2 NPs.

Interestingly, although we maintained the initial Bi-to-Pt atomic ratio in the precursors at a constant value of 1:2 for all temperatures, products with different phases were obtained at each temperature. However, when we varied the initial Pt-to-Bi atomic ratio at 260 °C, as long as the Bi-to-Pt ratio was no less than 1:1, only single-phase Pt_1Bi_1 was obtained. Similarly, at 350 °C, when the Bi-to-Pt ratio was no less than 2:1, only single-phase Pt_1Bi_2 was obtained regardless of the initial Bi-to-Pt atomic ratio. These results confirm that the reaction temperature exerts a strong influence on the phase of the products. When we varied the reaction temperature in the microfluidic reactor, phase control in the synthesis of the Pt−Bi intermetallic NPs was successfully and readily achieved.

The standard reduction potentials (SRPs) of pure Pt and Bi are +1.3 and +0.31 V, respectively.[13] Therefore, Pt^{4+} ions can be more quickly and readily reduced than can Bi^{3+} ions under the same conditions. When we added H_2PtCl_6 into the reaction solutions as the sole metal precursor and held the other conditions constant, pure Pt NPs were produced (Supporting Information Figure S3). However, when $Bi(NO_3)_3$ was used as the sole metal precursor, no change was observed in the solutions at the outlet of the microfluidic reactor, and no Bi NPs were obtained. This result suggests that $Bi(NO_3)_3$ alone cannot be reduced in the same solutions as those in which H_2PtCl_6 alone can be reduced. Therefore, we hypothesize that the mechanism for the formation of Pt−Bi intermetallic NPs might be as follows: the easily reduced Pt^{4+} ions are reduced first, and Pt seeds form; the Pt seeds thus formed induce or catalyze the reduction of Bi^{3+} ions; and when the reduction rate of Pt^{4+} ions and the induced reduction rate of Bi^{3+} ions equalize, ordered intermetallic compounds form, thus producing single-phase Pt_1Bi_1 or Pt_1Bi_2 at 260 or 350 °C, respectively. Conversion and co-reduction processes may be simultaneously involved in the formation of intermetallic NPs. A more detailed investigation is required to confirm this hypothesis.

The average size of the Pt_1Bi_2 intermetallic NPs prepared in ethylene glycol was 33.5 nm, as shown in Figure 3B; this is considerably larger than the optimum size reported for fuel cell catalysts.[2] Therefore, our subsequent studies were focused on decreasing the particle size of the Pt_1Bi_2 intermetallic NPs with the reaction temperature fixed at 350 °C. Various polyethylene glycols, such as PEG400 and PEG600, were also investigated for use as the solvents and reducing agents for the synthesis of Pt_1Bi_2 intermetallic NPs. The XRD patterns indicate that single-phase Pt_1Bi_2 was obtained for all solvents (Supporting Information Figure S4). The TEM images reveal that all products exhibited a spherical morphology, and the size distribution data illustrate that the particle size decreased as the molecular weight of the polyols increased (Supporting Information Figures S5−S7).

The average particle size was 33.5 nm for ethylene glycol, 19.2 nm for PEG400, and 13.2 nm for PEG600, suggesting that the particle size is dependent on the solvent. As the molecular weight increased, the viscosity of the polyols increased; consequently, the diffusion and growth processes involved in nanocrystal formation were significantly affected by the solvents.[15] In addition, the solvents also served as reducing agents, and the reducing capacity weakened as the molecular weight of the polyols increased. This observation indicates that tuning the solvents could allow for size control during the synthesis of the NPs, thus allowing a narrow particle size distribution to be achieved. Both the smallest average size and the narrowest size distribution were obtained using PEG600. The low-magnification TEM image of the product prepared in PEG600 that is presented in Figure 4A illustrates the large-scale production of Pt_1Bi_2 intermetallic NPs. As shown in the magnified TEM images (Figure 4B,C), the as-prepared Pt_1Bi_2 intermetallic NPs were spherical in shape and had an average size of 13.2 nm. Bright and dark regions can be clearly observed in the images of the spherical NPs. As shown in the inset of Figure 4C, the particles presented a knitted ball structure; the darker regions correspond to voids in the NPs. The HRTEM analysis presented in Figure 4D reveals lattice fringe distances of 0.614 and 0.224 nm, which can be indexed to the (001) and (11−2) planes, respectively, of Pt_1Bi_2.

To better understand the composition of the as-prepared intermetallic NPs, high-angle annular dark-field scanning transmission electron microscopy (HAADF-STEM) analysis

DOI: 10.1021/jacs.5b01088
J. Am. Chem. Soc. 2015, 137, 6263−6269

was performed. Figure 5 presents the EDS mapping images of the Pt_1Bi_2 intermetallic NPs, which show that the Pt and Bi

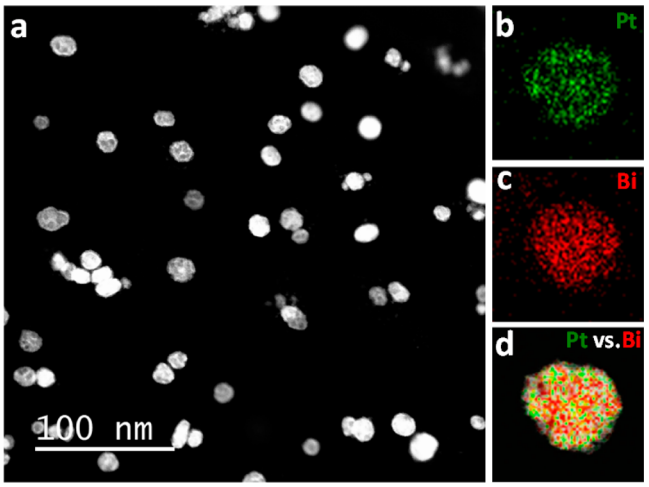

Figure 5. HAADF-STEM images and EDS element mapping images of Pt_1Bi_2 intermetallic NPs. (a) HAADF-STEM images of Pt_1Bi_2. (b_-d) HAADF-STEM-EDX mapping images.

were evenly dispersed throughout each individual Pt_1Bi_2 particle. This result indicates that the structures of the intermetallic compounds were homogeneous.

The influence of the capillary length on the particle size was also investigated. When the capillary length was decreased from 120 to 10 cm with the other conditions held constant, the size of the nanoparticles decreased to approximately 4 nm. The XRD, SEM and EDS results for Pt_1Bi_2 intermetallic nanoparticles prepared in a solution of PEG600 at 350 °C with a capillary length of 10 cm are presented in Supporting Information Figure S8.

Electrocatalysis of Pt−Bi Intermetallic NPs. Considering the economic factors for practical applications, we investigated the electrocatalytic performance of Pt_1Bi_2, which utilizes less Pt than does Pt1Bi1. To make the Pt_1Bi_2 intermetallic NPs into a practical electrocatalyst for a direct methanol fuel cell (DMFC), the Pt_1Bi_2 NPs were supported on Vulcan XC-72 carbon (Pt1Bi2/XC-72). The TEM images presented in Supporting Information Figure S9 show a fairly uniform distribution of the Pt_1Bi_2 intermetallic NPs on the carbon support.

The electrochemical performance of Pt_1Bi_2/XC-72 for the oxygen reduction reaction (ORR) was examined. The cyclic voltammograms of a commercial Pt/C catalyst and the Pt_1Bi_2/XC-72 catalyst in acidic electrolytes with and without methanol are shown in Supporting Information Figure S10. Figure 6 presents the ORR polarization curves of Pt_1Bi_2/XC-72, which were recorded in an O_2-saturated 0.1 mol/L $HClO_4$ solution using a rotating-disk electrode (RDE) at various rotation rates. A pretreatment process was applied to all electrodes by potential cycling between 0.0 and 1.2 V vs RHE at a sweep rate of 200 mV/s for 20 cycles to obtain a clean surface before the ORR activity was tested. The curves presented in Figure 6 demonstrate that the Pt_1Bi_2/XC-72 NPs possessed the ability to catalyze the reduction of O_2. An increase in the reduction current with increasing rotation rate was observed as a result of the improved diffusion of O_2 to the electrode surface.

This ORR enhancement in Pt_1Bi_2/XC-72 electrocatalysts may be attributable to the geometric and electronic structures of these catalysts. The Pt−Pt distance between nearest-

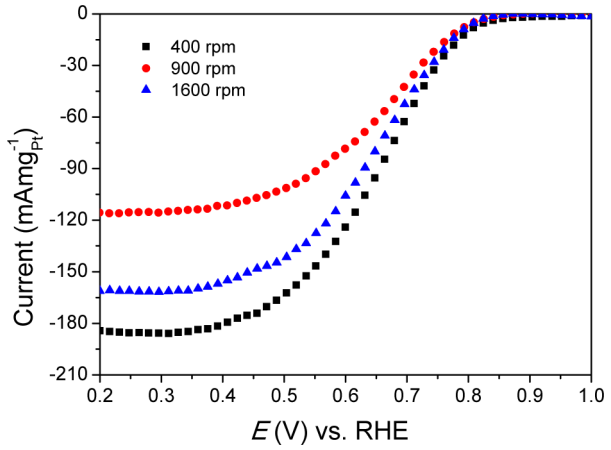

Figure 6. Polarization curves for the ORR on Pt_1Bi_2/XC-72 in O_2-saturated 0.1 mol/L $HClO_4$ at various rotation rates. Sweep rate: 10 mV/s.

neighbor Pt atoms is 0.278 nm for a monometallic platinum electrocatalyst,[1] whereas in ordered Pt_1Bi_2 intermetallic NPs, the closest Pt−Pt distance is 0.4739 nm.[6] The increased distance between Pt atoms in the intermetallic material will result in more favorable sites for enhancing the dissociative adsorption of oxygen. In addition, from the HRTEM image, we can observe that the as-prepared Pt_1Bi_2 NPs exhibited a knitted ball structure with the presence of voids, which improved the surface-to-volume ratio and increased the specific surface area, thereby contributing to the enhancement of the ORR electrocatalytic activity.

Pt−Bi intermetallic phases have been reported to possess excellent methanol tolerance.[17] To demonstrate the methanol tolerance of the Pt_1Bi_2 intermetallic NPs, we performed ORR tests in O_2-saturated 0.1 mol/L $HClO_4$ solutions that contained 0, 0.5, and 1.0 mol/L methanol at a rotation rate of 1600 rpm. Figure 7 compares the ORR polarization curves of Pt_1Bi_2/XC-72 and 20 wt % Pt/C, and it is evident that the onset potential and the oxygen reduction current density of the Pt/C catalyst were substantially decreased even in a low concentration of 0.5 mol/L methanol, whereas the corresponding values for Pt_1Bi_2/XC-72 remained nearly stable even at a high concentration of 1.0 mol/L methanol. At a current density of 45 mA/mg_{Pt}, the potential shifts from 0.85 down to 0.56 V with a large difference (0.29 V) for 20 wt % Pt/C, while the potential shifts from 0.64 to 0.62 V with a very small difference (0.02 V) Pt_1Bi_2/XC-72. These tests demonstrated that the as-prepared Pt_1Bi_2 intermetallic NPs possessed excellent methanol tolerance, which is important in DMFCs to eliminate the unwanted drop resulting from methanol crossover. The increased Pt−Pt distance in the Pt_1Bi_2 intermetallic NPs that results from the addition of Bi may contribute to preventing the formation of intermediate products during methanol oxidation, which, in turn, prevents the oxidation of methanol. Additionally, the Pt_1Bi_2 phase may result in charge redistribution that may subsequently lead to difficulty in forming oxygen-containing species from the dissociation of water.[17] The resistance of the Pt_1Bi_2/XC-72 catalyst to poisoning could significantly promote the development of commercial DMFCs.

To demonstrate the general applicability of microfluidic reactors in the synthesis of intermetallic nanomaterials, Pt_3Fe and Pt_1Sn_1 intermetallic NPs were also successfully prepared using the proposed method (Supporting Information Figures

DOI: 10.1021/jacs.5b01088
J. Am. Chem. Soc. 2015, 137, 6263−6269

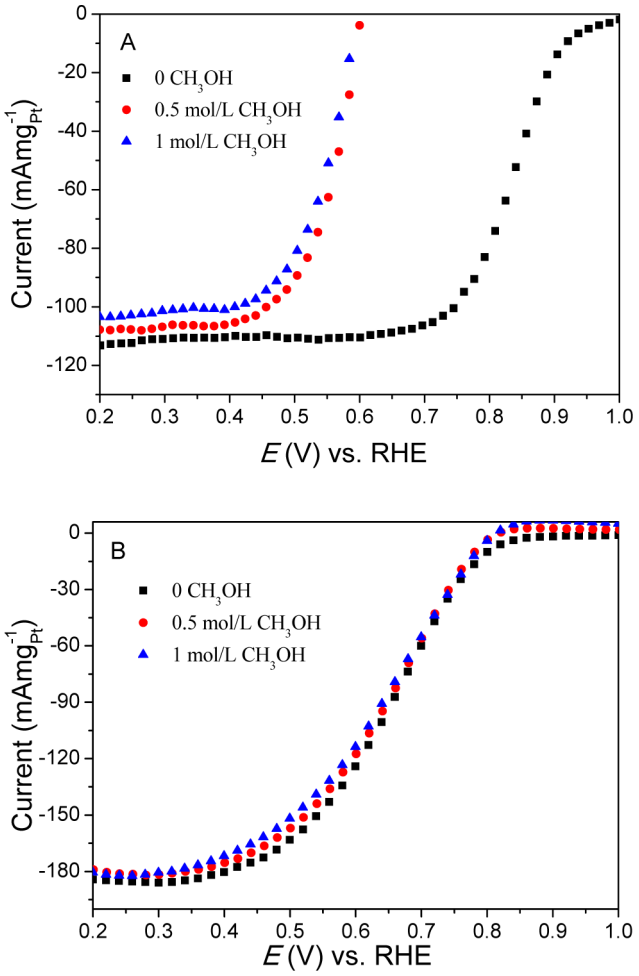

Figure 7. Polarization curves for the ORR. (A) Pt/C catalyst; (B) Pt_1Bi_2/XC-72 NPs. Conditions: in O_2-saturated 0.1 mol/L $HClO_4$ that contained 0, 0.5, and 1.0 mol/L methanol at a rotation rate of 1600 rpm. Sweep rate: 10 mV/s.

S11 and S12). Thus, we demonstrated the feasibility of preparing intermetallic NPs via a microfluidic synthesis strategy, which we hope will open new avenues toward the application of microfluidic technology in the synthesis of nanomaterials.

CONCLUSIONS

We presented a novel, ultrafast technique for the synthesis of intermetallic NPs using a one-step process based on a microfluidic strategy. The phase and size of the intermetallic NPs could be controlled by varying the reaction temperatures, the solvents and the length of the reaction channel. The synthesis process times were on the order of seconds. Pt−Bi intermetallic NPs were prepared as typical examples. When the reaction temperature was adjusted, pure Pt_1Bi_1 intermetallic NPs were formed at 260 °C, and Pt_1Bi_2 intermetallic NPs were obtained at 350 °C. When we varied the solvents, a series of Pt_1Bi_2 intermetallic NPs of different sizes were prepared, and the smallest-size NPs (average of 13.2 nm) were obtained using PEG600. The as-prepared Pt_1Bi_2 intermetallic NPs that were obtained from PEG600 were selected and loaded onto a XC-72 carbon support to act as an electrocatalyst for a DMFC, and the electrochemical performance of the catalyst indicated that it possessed a rather high ORR activity and excellent methanol tolerance. The proposed synthesis method was further extended to the successful preparation of other intermetallic nanomaterials, such as 8.6 nm-diameter Pt_3Fe and 6.3 nm-diameter Pt_1Sn_1 nanowires, to demonstrate its applicability and generality for a wide range of intermetallic NPs and its potential for application in other syntheses. Moreover, a study of the preparation of supported intermetallic NPs is currently in progress in our group and will be presented in forthcoming publications.

ASSOCIATED CONTENT

Supporting Information

Figure S1−S12, giving additional EDS, TEM images, XRD patterns, size distributions, and CV curves. The Supporting Information is available free of charge on the ACS Publications website at DOI: 10.1021/jacs.5b01088.

AUTHOR INFORMATION

Corresponding Authors

*xiayanwang@bjut.edu.cn
*dgxia@pku.edu.cn
*guogs@bjut.edu.cn

Notes

The authors declare no competing financial interest.

ACKNOWLEDGMENTS

This work was supported by the National Natural Science Foundation of China (NSFC) (No. 21375005, 21275014), the Excellent Young Scientists Fund of the NSFC (No. 21322501), the Importation and Development of High-Caliber Talents Project of Beijing Municipal Institutions (CIT&TCD20140309), the Program for New Century Excellent Talents in University (NCET-12-0603), and the Beijing Natural Science Foundation Program and Scientific Research Key Program of the Beijing Municipal Commission of Education (No. KZ201310005001). We thank Mr. Yan Wang of China Iron and Steel Research Institute Group for the discussion on electrochemical measurements.

REFERENCES

(1) Casado-Rivera, E.; Volpe, D. J.; Alden, L.; Lind, C.; Downie, C.; Vazquez- Alvarez, T.; Anglelo, A. C. D.; DiSalvo, F. J.; Abruna, H. D. *J. Am. Chem. Soc.* **2004**, *126*, 4043−4049.
(2) Ji, X. L.; Lee, K. T.; Holden, R.; Zhang, L.; Zhang, J. J.; Botton, G. A.; Couillard, M.; Nazar, L. F. *Nat. Chem.* **2010**, *2*, 286−293.
(3) Wang, D. L.; Xin, H. L. L.; Hovden, R.; Wang, H. S.; Yu, Y. C.; Muller, D. A.; DiSalvo, F. J.; Abruña, H. D. *Nat. Mater.* **2013**, *12*, 81−87.
(4) Mun, J. H.; Chang, Y. H.; Shin, D. O.; Yoon, J. M.; Choi, D. S.; Lee, K. M.; Kim, J. Y.; Cha, S. K.; Lee, J. Y.; Jeong, J. R.; Kim, Y. H.; Kim, S. O. *Nano Lett.* **2013**, *11*, 5720−5726.
(5) Wang, G. W.; Huang, B.; Xiao, L.; Ren, Z. D.; Chen, H.; Wang, D. L.; Abruña, H. D.; Lu, J. T.; Zhuang, L. *J. Am. Chem. Soc.* **2014**, *136*, 9643−9649.
(6) DeSario, D. Y.; DiSalvo, F. J. *Chem. Mater.* **2014**, *26*, 2750−2757.
(7) Casado-Rivera, E.; Gal, Z.; Angelo, A. C. D.; Lind, C.; DiSalvo, F. J.; Abruña, H. D. *ChemPhysChem* **2003**, *4*, 193−199.
(8) Volpe, D.; Casado-Rivera, E.; Alden, L.; Lind, C.; Hagerdon, K.; Downie, C.; Korzeniewski, C.; DiSalvo, F. J.; Abruña, H. D. *J. Electrochem. Soc.* **2004**, *151*, A971−A977.
(9) Oana, M.; Hoffmann, R.; Abruña, H. D.; DiSalvo, F. J. *Surf. Sci.* **2005**, *574*, 1−16.
(10) Alvarez, P.; Gorria, P.; Franco, V.; Marcos, J. S.; Perez, M. J.; Llamazares, J. L. S.; Orench, I. P.; Blanco, J. A. *J. Phys.: Condens. Matter* **2010**, *22*, 216005 (8pp).

DOI: 10.1021/jacs.5b01088
J. Am. Chem. Soc. 2015, 137, 6263−6269

(11) Takagiwa, Y.; Matsubayashi, Y.; Suzumura, A.; Okada, J. T.; Kimura, K. *Mater. Trans.* **2010**, *51*, 988−993.
(12) McDonald, J. P.; Rodriguez, M. A.; Jones, E. D.; Adams, D. P. *J. Mater. Res.* **2010**, *25*, 718−727.
(13) Sra, A. K.; Schaak, R. E. *J. Am. Chem. Soc.* **2004**, *126*, 6667−6672.
(14) Chou, N. H.; Schaak, R. E. *J. Am. Chem. Soc.* **2007**, *129*, 7339−7345.
(15) Cui, Z. M.; Chen, H.; Zhao, M. T.; Marshall, D.; Yu, Y. C.; Abruña, H.; DiSalvo, F. J. *J. Am. Chem. Soc.* **2014**, *136*, 10206−10209.
(16) Roychowdhury, C.; Matsumoto, F.; Mutolo, P. F.; Abruña, H. D.; DiSalvo, F. J. *Chem. Mater.* **2005**, *17*, 5871−5876.
(17) Roychowdhury, C.; Matsumoto, F.; Zeldovich, V. B.; Warren, S. C.; Mutolo, P. F.; Ballesteros, M.; Wiesner, U.; Abruña, H. D.; DiSalvo, F. J. *Chem. Mater.* **2006**, *18*, 3365−3372.
(18) Bauer, J. C.; Chen, X.; Liu, Q. S.; Phan, T. H.; Schaak, R. E. *J. Mater. Chem.* **2008**, *18*, 275−282.
(19) Liao, H. B.; Zhu, J. H.; Hou, Y. L. *Nanoscale* **2014**, *6*, 1049−1055.
(20) Xia, D. G.; Chen, G.; Wang, Z. Y.; Zhang, J. J.; Hui, S. Q.; Ghosh, D.; Wang, H. J. *Chem. Mater.* **2006**, *18*, 5746−5749.
(21) Song, Y. J.; Hormes, J.; Kumar, C. S. S. R. *Small* **2008**, *4*, 698−711.
(22) Abou-Hassan, A.; Sandre, O.; Cabuil, V. *Angew. Chem., Int. Ed.* **2010**, *49*, 6268−6286.
(23) Zhang, L.; Xia, Y. N. *Adv. Mater.* **2014**, *26*, 2600−2606.
(24) Zhang, L.; Niu, G. D.; Lu, N.; Wang, J. G.; Tong, L. M.; Wang, L. D.; Kim, M. J.; Xia, Y. N. *Nano Lett.* **2014**, *14*, 6626−6631.
(25) Elvira, K. S.; Solvas, X. C. I.; Wootton, R. C. R.; deMello, A. J. *Nat. Chem.* **2013**, *5*, 905−915.
(26) Song, Y. J.; Modrow, H.; Henry, L. L.; Saw, C. K.; Doomes, E. E.; Palshin, V.; Hormes, J.; Kumar. *Chem. Mater.* **2006**, *18*, 2817−2827.
(27) Boleininger, J.; Kurz, A.; Reuss, V.; Sonnichsen, C. *Phys. Chem. Chem. Phys.* **2006**, *8*, 3824−3827.
(28) Song, Y. J.; Zhang, T.; Yang, W. T.; Albin, S.; Henry, L. L. *Cryst. Growth Des.* **2008**, *8*, 3766−3772.
(29) Frenz, L.; El Harrak, A.; Pauly, M.; Begin-Colin, S.; Griffiths, A. D.; Baret, J. C. *Angew. Chem., Int. Ed.* **2008**, *47*, 6817−6820.
(30) Duraiswamy, S.; Khan, S. A. *Small* **2009**, *5*, 2828−2834.
(31) Lu, M. Q.; Yang, S. K.; Ho, Y. P.; Grigsby, C. L.; Leong, K. W.; Huang, T. J. *ACS Nano* **2014**, *8*, 10026−10034.
(32) Krishnadasan, S.; Tovilla, J.; Vilar, R.; deMello, A. J.; deMello, J. C. *J. Mater. Chem.* **2004**, *14*, 2655−2660.
(33) Yen, B. K. H.; Stott, N. E.; Jensen, K. F.; Bawendi, M. G. *Adv. Mater.* **2003**, *15*, 1858−1862.
(34) Edel, J. B.; Fortt, R.; deMello, J. C.; deMello, A. J. *Chem. Commun.* **2002**, *10*, 1136−1137.
(35) deMello, A. J. *Nature* **2006**, *442*, 394−402.
(36) Chan, E. M.; Mathies, R. A.; Alivisatos, A. P. *Nano Lett.* **2003**, *3*, 199−201.
(37) Kikkeri, R.; Laurino, P.; Odedra, A.; Seeberger, P. H. *Angew. Chem., Int. Ed.* **2010**, *49*, 2054.
(38) Krishna, K. S.; Li, Y. H.; Li, S. N.; Kumar, C. S. S. R. *Adv. Drug Delivery Rev.* **2013**, *65*, 1470−1495.
(39) Abou-Hassan, A.; Bazzi, R.; Cabuil, V. *Angew. Chem., Int. Ed.* **2009**, *48*, 7180−7183.
(40) Knauer, A.; Thete, A.; Li, S.; Romanus, H.; Csaki, A.; Fritzsche, W.; Kohler, J. M. *Chem. Eng. J.* **2011**, *166*, 1164−1169.
(41) Latham, A. H.; Williams, M. E. *Acc. Chem. Res.* **2008**, *3*, 411−420.
(42) Marre, S.; Jensen, K. F. *Chem. Soc. Rev.* **2010**, *3*, 1183−1202.
(43) Zhang, L.; Wang, Y.; Tong, L. M.; Xia, Y. N. *Nano Lett.* **2014**, *14*, 4189−4194.

DOI: 10.1021/jacs.5b01088
J. Am. Chem. Soc. 2015, 137, 6263−6269